International Journal of Impact Engineering 37 (2010) 521–529

Contents lists available at ScienceDirect

International Journal of Impact Engineering

journal homepage: www.elsevier.com/locate/ijimpeng

Behavior of portable fiber reinforced concrete vehicle barriers subject to blasts from contact charges

A.M. Coughlin [a,*], E.S. Musselman [b], A.J. Schokker [b], D.G. Linzell [c]

[a] Hinman Consulting Engineers, One Bush St., Suite 510, San Francisco, CA 94104, United States
[b] Department of Civil Engineering, University of Minnesota at Duluth, 1305 Ordean Court, Duluth, MN 55812, United States
[c] Department of Civil and Environmental Engineering, Protective Technology Center, The Pennsylvania State University, 212 Sackett Building, University Park, PA 16802, United States

ARTICLE INFO

Article history:
Received 27 July 2009
Received in revised form
29 August 2009
Accepted 6 November 2009
Available online 3 December 2009

Keywords:
Contact charge
Blast
Concrete barriers
Fiber reinforced concrete
LS-DYNA

ABSTRACT

Portable concrete barriers are commonly used to form a secure perimeter to prevent entry of terrorist vehicle borne improvised explosive devices (VBIEDs). Barrier effectiveness can be compromised when satchel charges are used to breach a protective perimeter and subsequently permit closer access to the intended target by VBIEDs. The behavior of five portable concrete vehicle barriers was tested under satchel sized contact charge explosives at the Air Force Research Labs (AFRL) test range at Tyndall Air Force Base, Florida. Four barriers representing different fiber reinforced concretes (FRCs) including two types of synthetic FRC, two steel-synthetic blend FRCs with different fiber volumes, and a traditional reinforced normal weight concrete which served as the control specimen. Each of the FRCs exhibited less material loss and surface damage compared to the control. The two steel synthetic blended concretes exhibited the least amount of damage of all barriers, with no visible difference in performance between the two fiber volumes. The control barrier had widespread spalling and limited concrete in the core of the specimen remained intact. A finite element model was created in LS-DYNA to model one FRC barrier and the control barrier to see if the models could predict the observed damage. Both models were deemed successful due to their ability to show similar patterns of damage as the tested barriers.

1. Introduction

Modern terrorist threats are constantly evolving and so must the systems used to mitigate them. In many locations impact resistant ("anti-ram") barriers are used to create a secure perimeter to prevent vehicle borne improvised explosive devices (VBIEDs) from detonating close to their intended targets. Increased standoff distance from a large explosion can prevent many casualties and loss of key assets since the magnitude of a blast decays rapidly as the distance from its center increases [1]. When a suitable anti-ram perimeter is in place, the size of explosive that can be detonated in close proximity to targets is limited. In certain cases, however, terrorist techniques have focused on first attacking a barrier with a hand carried explosive to breach it and allow a VBIED to detonate closer to the target, where the blast will have a more devastating effect.

Though anti-ram perimeters can take a variety of forms, portable massive concrete barriers, such as the ones tested in this study, are commonly used because of their versatility, low cost, and ease of construction. They can be implemented rapidly in high risk locations and rearranged when perimeter protection needs change. Concrete is a common material used for blast resistance due to its high mass per unit cost. However, its brittle nature makes concrete prone to spalling and fragmentation. It is well known that steel reinforcement can give concrete ductile behavior, however blast loads, especially those from close-in charges, can cause both reinforced and unreinforced areas to fail in a brittle manner.

Close-in blasts are less understood than far range blasts and can cause different response in concrete members [2]. Compared to far range blasts, close-in blasts have higher pressures, shorter load durations, and more temperature and gas clearing effects. As the standoff distance from a charge to a concrete panel is decreased, the blast can cause the panel to exceed a spall threshold, where fragments are ejected from the back of the panel. An even closer charge can cause the panel to exceed its breach threshold, where the blast is able to perforate the panel. The spall and breach thresholds have been observed empirically and have been shown to be dependent on concrete thickness and strength, but not on reinforcing percentage [2]. The explanation for these close-in effects is the propagation of compression waves causing areas of tensile failure

* Corresponding author. Tel.: +1 415 621 4423; fax: +1 415 621 4447.
E-mail address: andy@hce.com (A.M. Coughlin).

0734-743X/$ – see front matter © 2009 Elsevier Ltd. All rights reserved.
doi:10.1016/j.ijimpeng.2009.11.004

in the concrete. Far range blasts, which have longer load durations, are more likely to produce ductile flexural response in concrete members that are properly reinforced [3].

One method to reduce concrete spalling in blasts is through the use of fiber reinforced concrete (FRC) [3]. FRC is made by mixing discontinuous fibers into a concrete mix to achieve a somewhat uniform dispersion. Fiber materials such as steel, glass, carbon, polypropylene, and nylon have been used in FRC to achieve a variety of property enhancements, including: tensile strength; ductility; stiffness; crack resistance; durability; fatigue life; impact resistance; and shrinkage reduction [4]. It has also been shown to reduce spalling and increase fracture toughness in a variety of blast and impact applications when compared to normal concrete [5,6]. Fiber additives can also limit breach and spall velocity in blasts from close-in explosions [3] and allow concrete to develop additional tensile capacity by bridging tensile cracks when they form [7]. As fibers either pull out or yield, energy is absorbed and the fracture energy of the matrix is increased. Though these mechanisms explain the improved spall resistance in FRC, it is not well understood how behavior of FRC members under close-in blasts can be predicted.

The goal of this study was to measure blast performance improvements gained from FRC compared to traditional reinforced concrete in vehicle barriers when subjected to the blast from a contact charge. FRC barriers which stay intact after a blast from a contact charge could be a good choice for use in blast resistant portable concrete vehicle barriers. The primary performance goal of the barriers was to prevent vehicle entry after a blast and was measured in terms of loss of mass and extent of surface damage. The secondary performance goal was to minimize the amount of secondary fragmentation that could injure personnel. It was measured by mapping the debris field created from each barrier test. In addition to blast testing, a finite element modeling study was also completed to try to predict barrier damage of both traditional concrete and FRC barriers. Successful damage prediction would allow other barrier types to be assessed with less need for testing.

2. Blast testing

2.1. Barrier fabrication

Five concrete barriers were fabricated in an off-site casting facility and shipped to the testing range. General barrier drawings are shown in Fig. 1. The barriers were basically rectangular with exterior dimensions of 3050 × 1070 × 610 mm. They were reinforced with standard longitudinal and transverse bars and two steel plate tie bars used to chain the barriers together. The tie bars of adjacent barriers connected them together with a drop-in steel pin. This connection allowed the chain to achieve a greater anti-ram resistance than any individual barrier. Each barrier was assigned an identification code corresponding to its type of concrete, listed in Table 1.

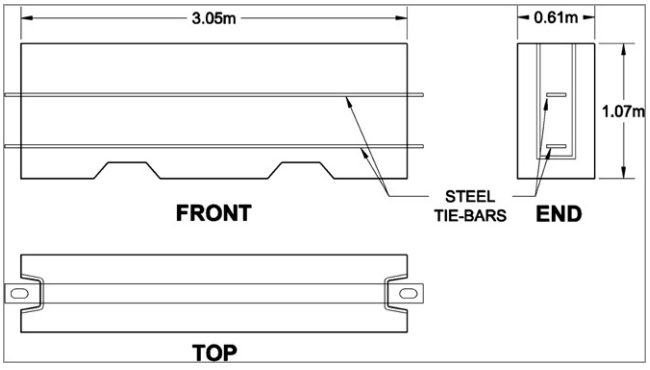

Fig. 1. Barrier drawings (not to scale).

Table 1
Barrier test matrix.

ID	Concrete
K-1	Standard Concrete (control)
CFRC	Carbon fiber
NFRC	Nylon fiber
SS–H	Synthetic/steel fiber mix 1 (high fiber volume)
SS–L	Synthetic/steel fiber mix 2 (lower fiber volume)

The control barrier (K-1) for the test was constructed with a 35 MPa minimum strength concrete mix commonly used by the fabricator. It consisted of 13 mm aggregate and a water to cement ratio of 0.39. Two barriers of fiber reinforced concrete, one with nylon fibers (NFRC) and the other with carbon fibers (CFRC), were constructed with 1.5% fibers by volume. The fibers were 75 mm in length and were given a special coating that gave the fibers higher initial rigidity and enabled good fiber dispersion during mixing [8]. The nylon and carbon fiber reinforced concrete mixes utilized silica fume blended cement and 9 mm pea gravel with a water to cement ratio of 0.34.

A mix of steel and synthetic fibers was used to construct barriers SS–L and SS–H with two different fiber volumes, 3.8% and 5% respectively. High modulus fibers (steel) were used to give the matrix a greater tensile strength the and low modulus fibers (polypropylene) were added to give greater energy absorption capacity in opening a crack [9]. Based on criteria presented by Naaman and Reinhardt [10] these mixes could be considered high performance fiber reinforced cementitious composites (HPFRCCs) because they exhibited displacement hardening in small scale beam tests. These mixes contained no course aggregates since at high fiber volumes it is often impossible to achieve a workable mix with course aggregate. Though cement mixes without course aggregate are technically considered mortars rather than concrete, for simplicity these mixes were grouped in the category with the other fiber reinforced concretes. The specific proportions of all concrete mixes are provided in Table 2.

Table 2
Barrier concrete mix designs.

IDs	K-1 (control)	CFRC, NFRC	SS–H, SS–L
Units	kg/m^3	kg/m^3	kg/m^3
Portland Cement	344	429	750
	Type I	Type I	Type I
Slag	86	184	–
Fly Ash	–	–	107
Fine Aggregate	831	628	1168
Course Aggregate	843	751	–
	13 mm aggregate	9 mm pea gravel	–
Water	169 L/m^3	209 L/m^3	313 L/m^3
Water Reducing Admixture	2200 ml/m^3	as needed	10,600 ml/m^3
Air Entrainment Admixture	270 ml/m^3	–	–
Set Retarder	–	–	270 ml/m^3
Fibers	–	[a]	[b, c]

[a] Carbon or nylon fibers added at 1.5% by volume.
[b] SS–H barriers included 30 mm flat end steel fibers at 2.5% by volume or 195 kg/m^3, 50 mm polypropylene/polyethylene fibers at 1.8% by volume or 16 kg/m^3, variable length polypropylene macro synthetic fibers at 0.6% by volume or 5 kg/m^3, and variable length polypropylene micro synthetic fibers at 0.066% by volume or 0.6 kg/m^3. Total fiber volume was 5.0%.
[c] SS–L barriers included 30 mm flat end steel fibers at 2.0% by volume or 156 kg/m^3, 50 mm polypropylene/polyethylene fibers at 1.33% by volume or 12 kg/m^3, variable length polypropylene macro synthetic fibers at 0.4% by volume or 4 kg/m^3, and variable length polypropylene micro synthetic fibers at 0.066% by volume or 0.6 kg/m^3. Total fiber volume was 3.8%.

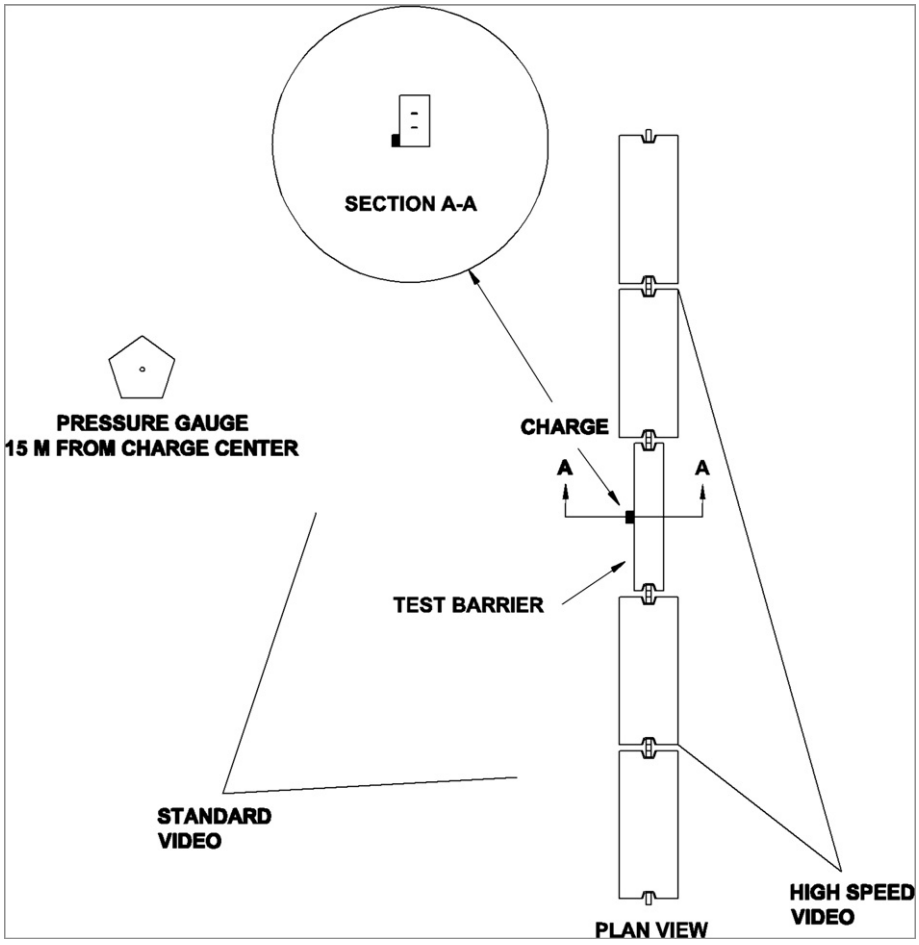

Fig. 2. Plan view of test setup.

2.2. Blast test procedure

Each barrier was tested at AFRL under air blast loading using C-4 explosives stacked at the base of the barrier. The exact weight of explosives cannot be disclosed due to the sensitive nature of this research. Each barrier was placed directly onto an on grade concrete slab and the slab was replaced after every test. The test barrier was connected in a chain to two support barriers on each side that were slightly larger but had similar mass due to their hollow cores. The barriers were connected with a steel pin through their tie bars. A free field pressure gauge located 15 m from the charge took continuous pressure readings during each test. Standard speed video was taken from the front and high speed video was taken from the rear. Besides video and pressure readings, no other data was collected during the test due to difficulty protecting instrumentation from blast heat and pressures. A diagram of the test configuration is shown in Fig. 2 and a photo of the arrangement before testing is given in Fig. 3.

After each blast test, the damage of each test barrier was documented with photographs of the front and rear of the barrier, close-up photographs of craters left by the blast, and overhead photographs of the debris field. Each test barrier's weight was

Fig. 3. Chain of barriers before testing.

Fig. 4. Control (K-1) barrier after test: front (left) and back (right).

Fig. 5. Carbon fiber barrier (CFRC) barrier after test: front (left) and back (right).

recorded prior to and after testing. The debris field was mapped for each barrier test using surveying equipment. Since hundreds of fragments were left from some blasts, only fragments with a 125 mm mean diameter or larger were mapped. The size and location of each fragment was recorded.

2.3. Blast test results

None of the barriers exhibited a complete breach, but their damage varied greatly. The control barrier, K-1, with most of its back face (away from the charge) ejected, sustained the greatest amount of damage. Large cracks extended radially outward from the center of the front crater and extended to a crater on the top of the barrier. The crater extended throughout the majority of the back face. The transverse steel reinforcing failed where the hoops lapped at the bottom. Most of the remaining concrete in the interior of the barrier was reduced to fragments held together by the steel tie bars. Light could be seen between the fragments suggesting that there was no remaining concrete continuity. Front and rear elevation photos of damaged barrier K-1 are shown in Fig. 4.

The carbon and nylon fiber reinforced concrete barriers (CFRC and NFRC) sustained similar patterns of damage as the control, but to a lesser extent. Cracks around the front crater were similar to the control barrier, however, a large vertical crack extended to the top of the barrier and no concrete was missing from the top. A large crater was observed on the back of each barrier, but the interior concrete appeared much more intact, blocking all light from passing through. Elevation photos of these barriers are shown in Fig. 5 and Fig. 6.

The two steel synthetic blended fiber barriers (SS–L and SS–H) had a similar behavior as the FRC barriers, except their rear craters were smaller and damage was less extensive. The difference in fiber volume between these two barriers seemed to have little effect. Their elevation photos are shown in Fig. 7 and Fig. 8.

The extent of the damage to each barrier was quantified graphically by mapping the craters on the front and back faces and comparing the crater area, A_1, to the total area, $A_1 + A_2$. This is demonstrated in Fig. 9. The percent of surface damage was calculated by $100\% \times A_2/(A_1 + A_2)$. The results are plotted in Fig. 10. In addition to this, weights of the barriers were taken before and after the test to calculate the mass of ejected concrete material. The results of these measurements are shown in Fig. 11.

In general, less damage was observed with an increase in fiber volume, though no reduction in damage was observed when fiber volume increased from 3.8% to 5%. Carbon fiber and nylon fiber barriers had very similar amounts of damage. All the FRC barriers, however, showed dramatic reduction in damage compared to the control barrier.

Secondary debris fields from each damaged barrier were mapped to study trends in the size and speed of fragments ejected from the barriers. Both small and large concrete fragments can threaten bystanders during a blast. Flying concrete fragments are more dangerous if they are large and have high velocities. Large fragments are more likely to cause injuries and fatalities than smaller fragments, though small fragments can still seriously threaten bystanders. Though the actual velocities of the fragments were not measured, the distance of each fragment from the charge center correlates to its exit velocity since fragments with a greater exit velocity generally fly farther. The number of fragments with a mean diameter of 125 mm or larger that were located further than 15 m, 30 m, and 45 m are plotted for each test in Fig. 12.

Results showed that every FRC barrier had higher numbers of fragments falling past the 15 m, 30 m, and 45 m lines than the control barrier [11]. Despite losing the most concrete mass, the

Fig. 6. Nylon fiber (NFRC) barrier after test: front (left) and back (right).

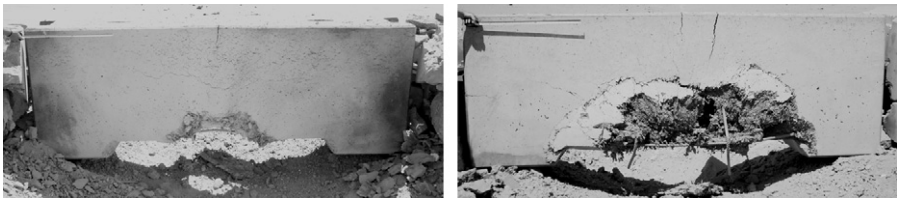

Fig. 7. Low volume steel/synthetic fiber (SS–L) barrier after test: front (left) and back (right).

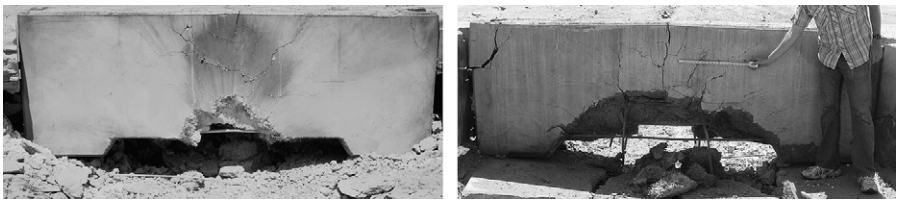

Fig. 8. High volume steel/synthetic fiber (SS–H) barrier after test: front (left) and back (right).

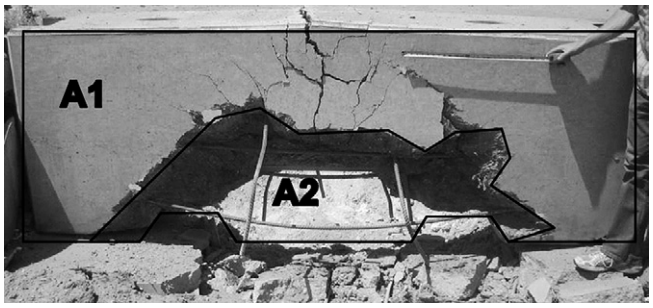

Fig. 9. Example of damage mapping on barrier.

control barrier tended to separate into much smaller fragments than the FRC barriers. The carbon FRC barrier had the highest number of fragments landing past all three distances. The nylon FRC barrier had roughly one third the fragments as the carbon FRC barrier despite having the same fiber volume (1.5%). It is postulated that the carbon fibers, which were flat, had a higher surface area than the nylon fibers, which were in a bundle, giving fragments greater cohesiveness. The steel/synthetic FRC with 5% fiber volume (SS–H) had a higher number of fragments than that with 3.8% fiber volume (SS–L). The larger volume of fibers was the likely reason for the increase in fragments, since additional fibers would hold more fragments together.

3. Finite element modeling

3.1. Model description

The finite element code LS-DYNA [12] was used to model the control barrier (K-1) and the carbon fiber reinforced concrete barrier (CFRC) using explicit time step integration. Models were developed to test whether analytical results would match results of experimental testing. Barriers K-1 and CFRC were chosen because their material properties had been well characterized from previous laboratory testing [8]. A half-symmetry model was used that included one support barrier and one-half of a test barrier, utilizing a plane of symmetry through the midline of the test barrier. Forklift pockets in the tested barriers (Fig. 1) were not modeled for the sake of simplicity. Solid 8-noded hexahedron elements were used to mesh the concrete, 4-noded shell elements were used to mesh the steel tie bars, and linear 3-noded Belytsckcho-Schwer beam elements [12] were used to model the longitudinal and transverse reinforcing bars. The support barriers were discretized into 75 mm cube solid elements and the test barrier was discretized into 25 mm cube elements. Perfect bond was assumed between the concrete and all embedded steel. The model was supported and constrained using a rigid surface contact definition at the location of the ground having a coefficient of

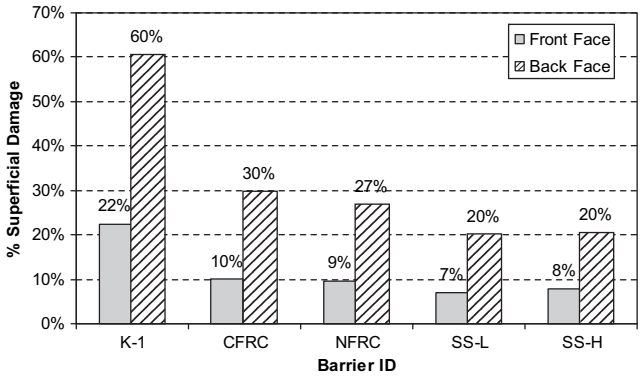

Fig. 10. Surface damage of front and back faces of barriers.

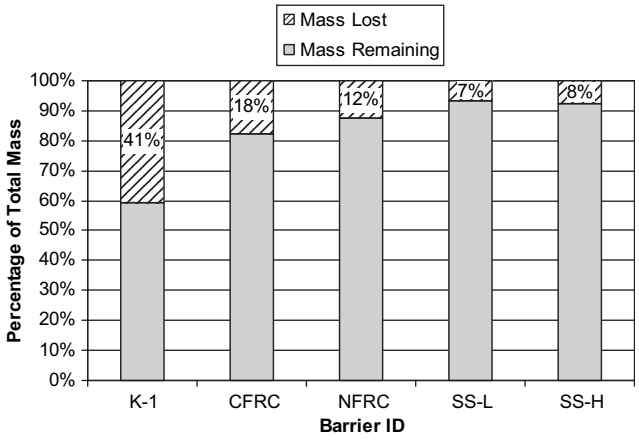

Fig. 11. Percentage of barrier material ejected during blast.

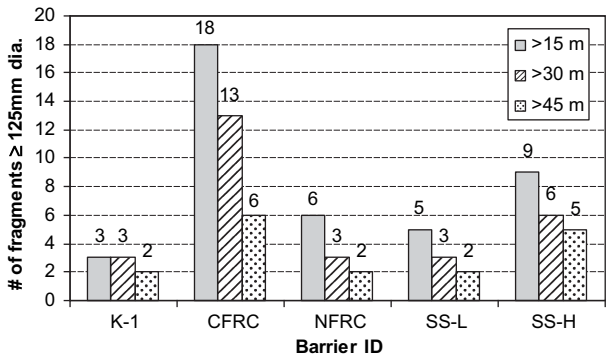

Fig. 12. Debris fragments Greater than 125 mm mapped from each barrier.

friction of 0.3. The tie bars between the barriers were given merged nodes at the locations of the drop-in pin to give connectivity between adjacent barriers. The outside of the support barrier was given nodal constraints at its tie bars in both horizontal directions to give restraint to the model.

The charge center and equivalent weight of TNT used to apply the blast load to the models was defined using the *LOAD_BLAST function in LS-DYNA [13]. This function calculates blast pressure time histories for a set of surfaces based on charts in the US Army Technical Manual 5-855-1: *Design and Analysis of Hardened Structures for Conventional Weapons Effects* [2]. All faces of the barrier model were defined to receive pressures from the blast load. A factor of 1.28 was used to convert the mass of C-4 to the equivalent mass of TNT, which corresponded to the average of the reported ratios of peak pressure and peak impulse measured from detonations of the two types of explosives [2].

The selected steel material model was a bilinear stress strain curve including strain rate effects using expected yield and ultimate strengths of ASTM A615M Grade 420 reinforcing steel, 475 and 750 MPa, respectively [14]. A triaxial damage model, the Continuous Surface Cap Model (CSCM) [15], was used to model concrete in the barriers. The CSCM model was developed for the United States Federal Highway Administration to model crashworthiness of concrete transportation structures. It was shown by Magallanes [16] to accurately predict the response of several types of concrete

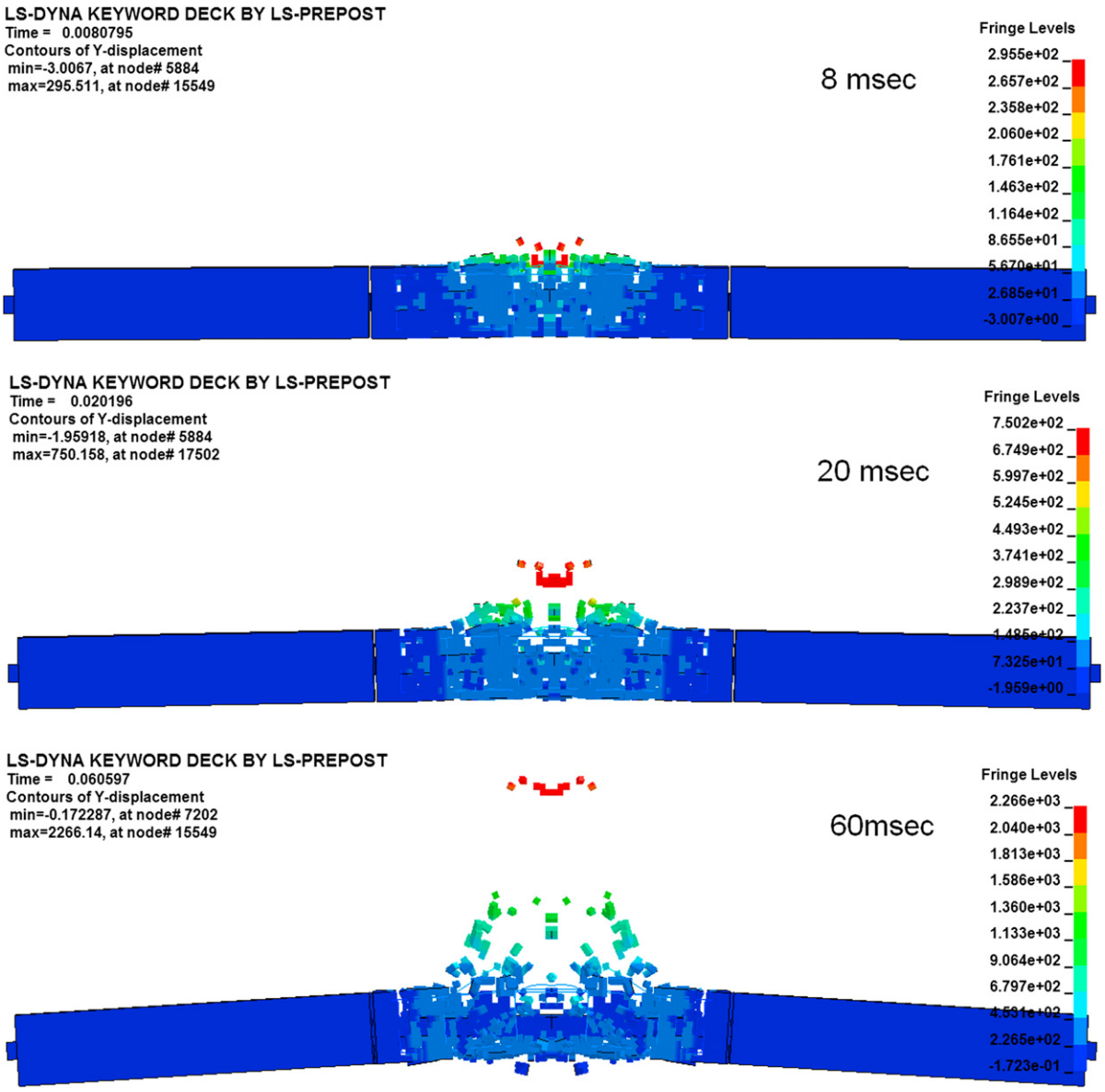

Fig. 13. Top view of K-1 barrier with displacement contours (mm).

elements exposed to blast loads. The CSCM model was chosen over the Concrete Damage Model (Material 72) [17] because single element tensile model runs showed tensile strain softening curves that more closely resembled data from uniaxial tensile tests of carbon fiber reinforced concrete [8]. Material parameters were automatically generated in LS-DYNA from the target concrete compressive strength of 45 MPa based on a library of concrete triaxial test data. The CFRC barrier model used the same material parameters as the control concrete, but the fracture energy parameters for tension and shear were modified to match the results of previous uniaxial tensile tests [8]. Default strain rate parameters were that were used corresponded to values given in the European CEB code [18]. To track damage to the barriers as the blast event progressed, a damage-based erosion function was invoked to delete elements which reached a 99 percent damage threshold.

3.2. Modeling results

Finite element model results showed widespread element erosion in the control barrier (K-1), representing spalling and cracking of the concrete. More spalling was observed in the control model than in the carbon FRC model. After 100 ms, 80% of elements had eroded in the control model compared to only 19% in the CFRC model. Damage in the carbon FRC model was limited to the middle third of the barrier width on the front and back faces. Concrete solid elements were ejected from both models, though the spall from the control barrier left at a higher velocity than the spall from the carbon FRC barrier. Top views of the barrier models are shown in Fig. 13 and Fig. 14 respectively.

To validate the model, the front and back craters from both modeled barriers were mapped and compared with the mapped craters from the actual damaged barriers. The damaged area was defined as the locations where the outside elements had eroded. The border between the remaining outside elements and the area of damage is shown in Fig. 15 for barrier K-1 and Fig. 16 for barrier CFRC. Table 3 shows a comparison of the surface damage measured experimentally and predicted analytically for barriers K-1 and CFRC. The percentage difference between the analytical and experimental barriers was at most 54%, a very reasonable prediction given the unpredictable nature of blasts.

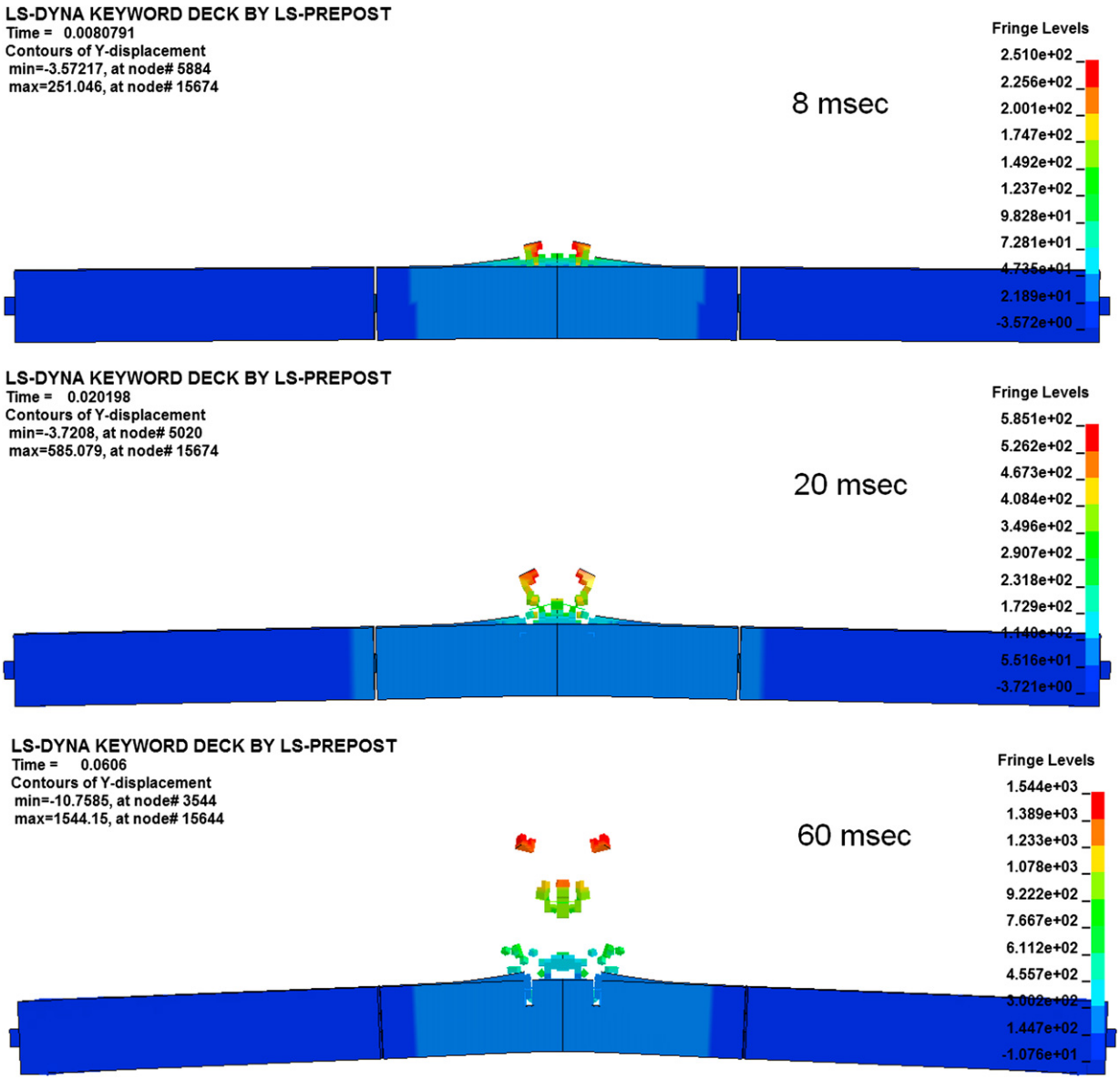

Fig. 14. Top view of CFRC barrier with displacement contours (mm).

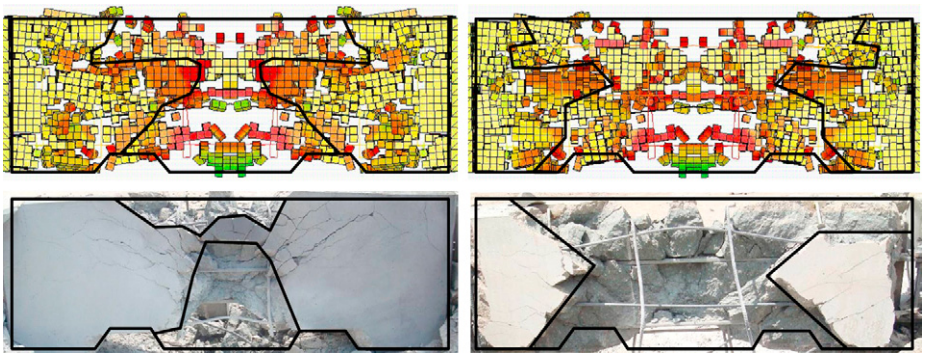

Fig. 15. Comparison of front (left) and back (right) crater mappings from analytical and experimental studies, barrier K-1.

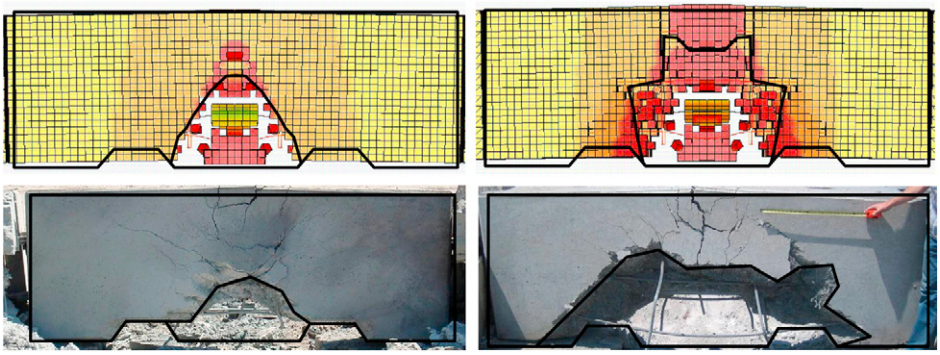

Fig. 16. Comparison of front (left) and back (right) crater mappings from analytical and experimental studies, barrier CFRC.

Table 3
Comparison of surface damage from experimental and analytical studies.

Barrier	Face	% of Surface damaged			% Difference
		Experimental	/	Analytical	
K-1	Front	22.2%	/	38.5%	54%
	Back	60.4%	/	62.2%	3%
CFRC	Front	9.8%	/	12.1%	21%
	Back	29.8%	/	22.7%	27%

Though close-in blasts can be difficult to model, these relatively simple three-dimensional models, constructed in LS-DYNA using simple geometry, readily available material models, and empirically derived blast loads, were shown to predict the damage a barrier sustained reasonably accurately. The models also showed that a concrete material without well defined properties could be modeled with reasonable accuracy under blast loads by incorporating the results of several small scale laboratory tests. While the models that were developed are not exact, they are simple to implement and can be utilized when blast testing is not a feasible option to test a barrier's performance.

4. Conclusions

The conclusions taken from this study are as follows:

- Fiber reinforced concrete limits the extent of damage and keeps damaged concrete more intact than normal concrete in barriers exposed to contact charges. Traditional concrete was much more likely to become fragmented, which would greatly reduce its resistance to vehicle impact.
- Nylon fiber reinforced concrete barriers at 1.5% fiber volume, the smallest increase in fiber volume that was studied, were shown to give great improvement in performance over typically reinforced concrete barriers, in terms of reduction of mass lost and superficial damage.
- The 3.8% steel/synthetic fiber mix (SS–L) performed to the same level as the 5% mix of the same fibers (SS–H), showing there is little performance improvement from increased fiber volume when fiber volume is already at a certain level. The fiber volume level where additional fibers do not result in performance improvements will likely occur below 3.8% for a steel/synthetic fiber blend concrete.
- Higher fiber surface area was found to increase the prevalence of large fragments in the debris field by holding debris together, resulting in increased fragment sizes.
- Development and implementation of a relatively simple finite element model in LS-DYNA and examination of select barrier responses under empirically based blast loading showed reasonably good agreement for barrier damage patterns when compared with blast test results for both a traditional and fiber reinforced concrete specimen. This makes finite element modeling an attractive alternative when blast testing is not feasible.

References

[1] Departments of the Army, the Navy, and the Air Force. Structures to resist the effects of accidental explosions TM 5-1300. Washington DC: Departments of the Army, the Navy, and the Air Force; 1990.
[2] Departments of the Army, the Navy, and the Air Force. Design and analysis of hardened structures to conventional weapons effects TM 5-855-1. Washington DC: Departments of the Army, the Navy, and the Air Force; 1986.
[3] McVay MK. Spall damage of concrete structures technical report SL-88-22. Vicksburg, MS, USA: US Army Corps of Engineers; 1988.
[4] ACI Committee 544. Report on fiber reinforced concrete ACI 544.1R-96 (Reapproved 2002). Farmington Hills, MI, USA: American Concrete Institute; 1996.

[5] Lan S, Lok TS, Heng L. Composite structural panels subjected to explosive loading. Construct Build Mater 2005;19:387–95.
[6] Luo X, Sun W, Chan SYN. Characteristics of high-performance steel fiber-reinforced concrete subject to high velocity impact. Cement Concr Res 2000;30:907–14.
[7] Bentur A, Mindess S. Fibre reinforced cementitious composites. 2nd ed. London: Taylor and Francis; 2007.
[8] Musselman E. Blast and impact resistance of carbon fiber reinforced concrete. Ph.D. dissertation. (advisor Andrea Schokker), The Pennsylvania State University, University Park, Pennsylvania, USA; 2007.
[9] Maalej M, Quek ST, Zhang J. Behavior of hybrid-fiber engineered cementitious composites subjected to dynamic tensile loading and projectile impact. J Mater Civil Engg 2005;17(2):143–52.
[10] Naaman AE, Reinhardt HW. Proposed classification of HPFRC composites based on their tensile response. Construction materials. In: Proceedings of the 3rd international conference on construction materials: performance, innovations and structural implications – ConMat '05 and Mindess Symposium. Vancouver (BC, Canada): The University of British Columbia, 2005. p. 458.
[11] Coughlin A. Contact charge blast performance of fiber reinforced and polyurea coated concrete vehicle barriers. Master's thesis. (advisors Andrea Schokker and Daniel Linzell), The Pennsylvania State University, University Park, Pennsylvania, USA; 2008.
[12] Lawrence Software Technology Corporation. LS-DYNA keyword user's manual, version 971. Livermore, CA, USA: Livermore Software Technology Corporation; 2007.
[13] Randers-Pehrson G, Bannister KA. Airblast loading model for DYNA2D and DYNA3D ARL-TR-1310. Adelphi, MD, USA: Army Research Laboratory; 1997.
[14] Malvar LJ. Review of static and dynamic properties of steel reinforcing bars. ACI Mater J 1998;95(5):609–16.
[15] Murray YD. Users manual for LS-DYNA concrete material model 159 Report No. FHWA-HRT-05-062. Washington DC: Federal Highway Administration; 2007.
[16] Magallanes JM. Importance of concrete material characterization and modelling to predicting the response of structures to shock and impact loading. In: Jones N, Brebbia CA, editors. Structures under shock and impact X, WIT transactions on the built environment 98. Algarve, Portugal: WIT Press; 2008. p. 241–50.
[17] Malvar LJ, Crawford JE, Wesevich JW, Simons D. A plasticity concrete material model for DYNA3D. Int J Impact Eng 1997;19(9–10):847–73.
[18] Comité euro-international du béton. CEB-FIP model code 1990 design code. London: T. Telford; 1993.